Available on CMS information server **CMS CR 1999/030**

CMS Conference Report

7 December 1999

Physical modeling of silicon microstrip detectors: influence of the electrode geometry on critical electric fields.

D. Passeri, A. Scorzoni

Dip. di Ingegneria Elettronica e dell'Informazione, Università di Perugia, Via Duranti 93, 06131 Perugia, Italy

P. Ciampolini

Dip. di Ingegneria dell'Informazione, Università di Parma, Parco Area delle Scienze 181/A, 43100 Parma, Italy

G. M. Bilei

INFN - Sezione di Perugia, Via A. Pascoli 1, 06100 Perugia, Italy

Abstract

In this paper, a computer-based analysis of AC-coupled silicon microstrip detectors is presented. The study aims at investigating the main geometrical parameters responsible for potentially critical effects, such as early micro-discharges and breakdown phenomena. The adoption of CAD tools allows for evaluating the actual field distribution within the device, and makes it possible to identify critical regions. The adoption of overhanging metal strips is shown to have a positive impact on the electric field distribution, reducing corner effects and thus minimizing breakdown risks.

Presented at *IEEE Nuclear Science Symposium*, Seattle, WA (U.S.A.), October 24-30, 1999

Submitted to *IEEE Transactions on Nuclear Science*

1 Introduction

Silicon microstrip detectors are being widely used within vertex detectors used in High Energy Physics (HEP) experiments: their exploitation in future, high-luminosity colliders, however, requires some issues concerning radiation hardness to be carefully considered. Progressive radiation damage suffered by operating detectors, in fact, influence their performance with many respects: most notably, bulk defects are introduced, acting as deep-level carrier traps, and thus eventually resulting in the type-inversion phenomenon. This, in turn, lowers the charge collection efficiency of detectors [1]. Oxide-trapped charge increases with the radiation as well, resulting in an increase of the parasitic interstrip capacitance. In order to compensate for the performance degradation induced by the radiation, the detector bias voltage need to be progressively increased (so that full-depletion can be eventually attained anyway). This is indeed an effective mean to preserve performance of the detector throughout its active life [2]: however, when increasing the reverse-bias voltage, leakage currents increase as well; apart from implying larger power and heat dissipation, this may significantly worsen the S/N ratio. In particular, it should be noted that such an increase in the leakage current is not uniformly distributed within the bulk, but, instead, it shows up earlier at some geometrical singularities of the structure. This results in a sudden increase of the strip noise, which possibly occurs at bias voltages well below the junction breakdown voltage.

Therefore, in order to optimize the detector design, it is of the utmost importance to identify regions at which leakage may preferentially develop, and to correlate the threshold of such phenomenon to geometrical and physical device characteristics. This can be done in a relatively fast and inexpensive way by means of computer simulation techniques. In this paper, we discuss the application of CAD device-analysis tools to investigate the influence of the shape of the aluminum layer in AC-coupled microstrip detectors on the noise coming from localized micro-discharges. The adoption of an "overhanging" metal contact, projecting itself beyond the strip implant boundary, has been proposed as an help in keeping under control the critical bias in heavily irradiated detectors [3]. Our study provides a physical interpretation to this observation, and allows for evaluating sensitivity to most design parameters. In Section II below, basic features of the simulation environment are summarized, whereas simulation results are discussed in Section III. Conclusions are eventually drawn in Section IV.

2 The simulation technique

Solid-state semiconductor detectors are modeled at a physical, distributed level by using a general-purpose device simulator [4]. The program solves the semiconductor transport equations (in the drift-diffusion approximation) over a discretized two-dimensional domain, and it has been customized for the analysis of radiation detectors. In particular, features relevant to this goal include: *i)* a transient-simulation mode dedicated to the charge-collection analysis [5], and, *ii)* a physically accurate model of bulk radiation damage, based on multiple deep-level traps [6]. Moreover, thanks to the discretization scheme adopted, the tool features a high flexibility in the geometrical description of the simulation domain: this makes it possible to quickly analyze responses coming from different device designs, and to correlate the actual device shape to its electrical characteristics. In this case, being interested in the onset of the breakdown or micro-discharge currents, the tool has been used to estimate the electric field distribution, looking for critical regions (i.e., regions of localized, intense field) and for geometrical details having some influence on them.

Basic features of the simulated devices are sketched in Fig. 1: it represents a cross-section of a two-strip subset of a single-sided microstrip array. p^+ strip implants are grounded through an ohmic contact (not shown in the figure) and are AC-coupled to the aluminum gate deposited onto an oxide-nitride sandwich. Depletion is attained by positively biasing the back ohmic contact. A thicker oxide fills the interstrip gap: to investigate the actual field distribution, different extensions of the metal layer over the thick oxide (the "overhang" of the metal contact), as well as different strip widths and pitches have been considered. Since, in this case, fringing effects are expected to play a significant role, a non-ideal field boundary-condition at the device surface has been taken into account: a free-air layer above the oxide has been included in the simulation domain, thus allowing for a more realistic description of fringing field-lines.

3 Simulation results

A first simulation result is shown in Figs. 2 and 3, which compare the electron distribution in the subregion (a) (see Fig. 1), for a device featuring no overhang and a 12μm-wide overhang, respectively. It has been shown elsewhere [6] that the oxide- and the interface-trapped charge are responsible for the shallow majority-carrier accumulation layer in the interstrip region, clearly visible on the left, front side of Figs. 2 and 3. Such a layer is still present

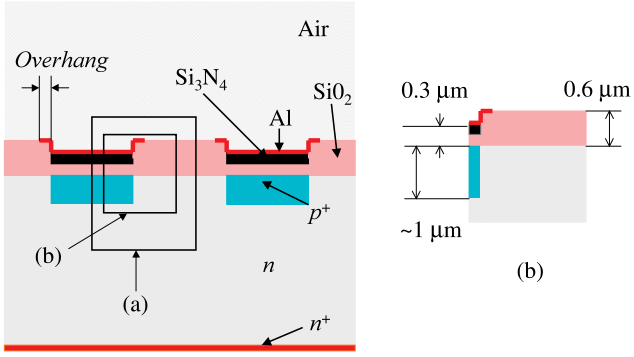

Figure 1: View of the simulated structure.

even at full-depletion voltages, and usually dominates the interstrip capacitance. When the overhanging contact is present, however, it acts there as a p-channel MOS gate, which, under the given bias conditions, suppresses the accumulation layer and tends to deplete the underlying region. This indicates a deep change in the electric field profile at the edge of the p^+ implant, depending on the overhang extension.

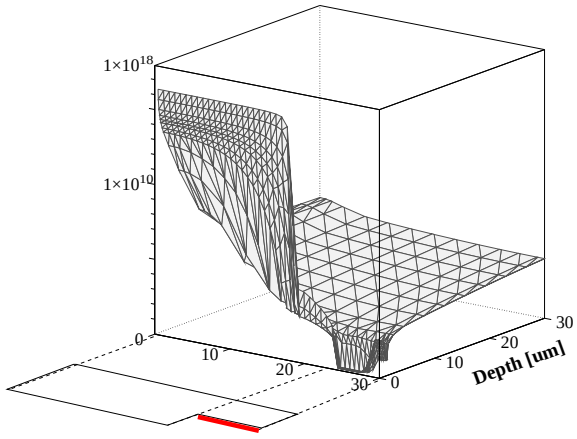

Figure 2: Electron concentration within subregion (a), no metal overhang.

At a first glance, the effect of increasing the extension of the metal contact significantly enhances the electric field amplitude within the silicon oxide, as illustrated in Fig. 4. Nevertheless, due to the much higher breakdown-critical fields, discharge phenomena within the oxide are not of practical concern, at least within the usual operating voltage range of silicon detectors.

On the other hand, a sensible decrease of the electric field amplitude within the silicon substrate is predicted by the simulation: it may therefore be useful to look in deeper detail at the field distribution there. In Fig. 5 a set of simulation results is compared: each sub-figure shows a contour plot of the electric field modulus within a region close to the strip implant, corresponding to the subregion (b) in Fig. 1. Dependence of the electric field on three geometrical parameters has been taken into account: namely, the sensitivity of the "maximum" field on the extension of the contact overhang, on the implant width (W) and on the strip pitch (P) have been investigated. To discuss these results, let us first refer to the simpler case of no-overhanging structures (the upper row in each subfigure): all the plots show the same qualitative behavior, featuring a field peak located at the p^+ edge, were field lines due to the reverse-biased junction and to the fringing action of the metal gate converge. By comparing the plots, it appears that horizontally scaling up the structure, both in width and pitch, results in an increase of the peak field, whereas increasing the W/P ratio, instead, reduces such a peak. This behavior can be easily interpreted by looking at the fringing capacitance between the strip and the backplane contact: we can assume such a fringing capacitance to arise from the coupling of the strip "corner" and the part of the backplane contact which lies outside

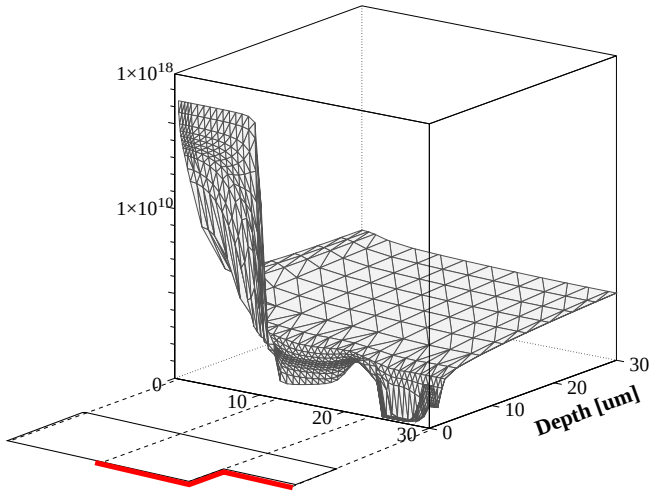

Figure 3: Electron concentration within subregion (a), metal overhang 12 μm.

of the strip vertical "footprint" (Fig. 6). The geometry of the first "plate" of the sidewall capacitor (being it a "corner") scarcely depends on the actual strip width and pitch, whereas, by accounting for the structure symmetry, the backplane plate can be roughly estimated to be $(P-W)/2$ wide. Field lines departing from such a plate tend to concentrate at the upper corner: such an effect is responsible for the field peaks discussed above, which therefore, at first order, depends on $(P-W)/2$. For instance, by keeping P constant and increasing the W/P ratio (i.e., moving along a horizontal row in the plot array of Fig. 5) and considering that:

$$\frac{P-W}{2} = \frac{P}{2}\left(1-\frac{W}{P}\right)$$

it turns out that the fringing capacitor extension decreases, as well as the peak electric field. On the other hand, by increasing W and P of the same amount, the difference $(P-W)$ increases proportionally, thus resulting in the peak field enhancement which can be appreciated by moving upward along a column in the plot array of Fig. 5.

A qualitatively similar behavior is preserved when some overhang is accounted for, as shown in the remaining plots. Increasing the overhang extent results, however, in an electric field redistribution, the main features of which can be quite easily interpreted. The fringing effect discussed above is due to the convergence of field lines, which come from the backplane contact and point toward the strip "corner". Actually, such a corner consists of a somehow more articulated structure: both the p^+ implant and the metal electrode edges contribute to the sidewall geometry. By projecting the metal strip edge beyond the implant boundary, these corners are misaligned, and field lines are "diluted" within a wider spatial extension.

The influence of the metal contact overhang can be perhaps more easily understood by looking at the potential contour plots in Fig. 7: the action of the overhang, which "pushes" the potential gradient away from the implant corner can be straightforwardly appreciated there.

Eventually, at larger overhangs, two almost separate corner effects become visible, each being responsible for a field peak: nevertheless, the overall field distribution is definitely milder and, therefore, less critical with respect to breakdown issues. Of course, such a beneficial effect is more effective for the critical geometrical configurations discussed above, i.e., those featuring wider interstrip spacings. This can be directly evaluated by looking at Fig. 8, in which the peak electric field amplitude is correlated to the overhang extension and to the strip geometrical configurations.

From these plots, a significant decrease (up to 40%, within the considered range) of such a peak amplitude can be inferred. The simulation also predicts some saturation of this effect, i.e., further extension of the overhang are expected to act less efficaciously.

Our analysis has been extended to irradiated detectors: breakdown phenomena, in fact, are more likely to occur on aged detectors, due to the need of compensating radiation damage with increasing reverse-bias voltages. In this case, however, one could expect that, once the substrate type-inversion has been reached, the corner effects discussed so far should become less important, since the "effective" junction has migrated at the backplane ohmic contact, which features no geometrical singularities.

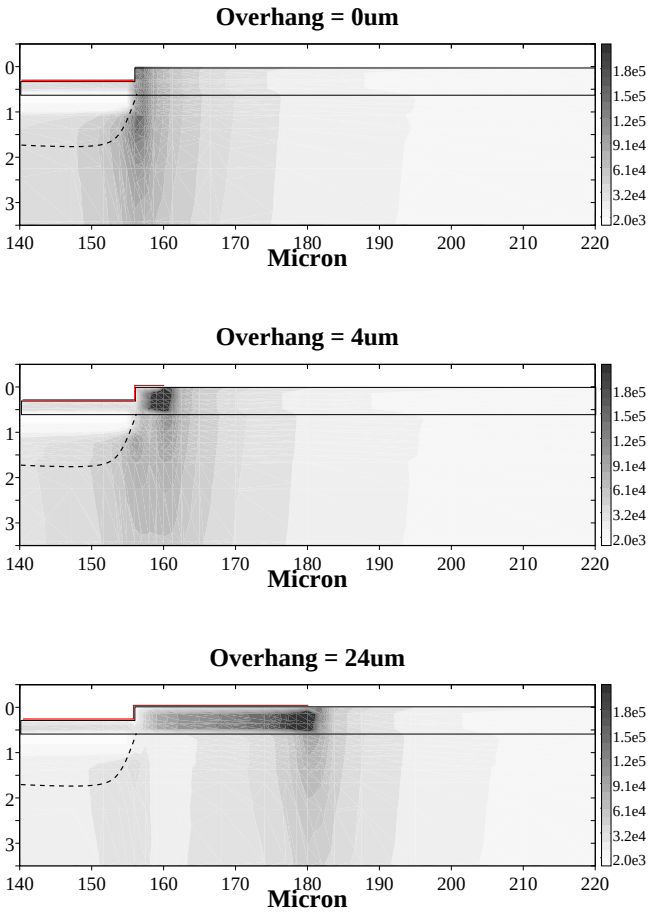

Figure 4: Electric field distribution. Implant width=72 μm, pitch=240 μm, V_{bias}=250V.

Simulations, however, contradict such a view: in Fig. 9, the field distribution close to the strip implant is illustrated, as predicted for irradiated structures. Actually, electric field peaks are still predicted there, even at fluences well beyond the type-inversion dose. This can be understood if a detailed account of the carrier trapping mechanisms is given: within our CAD environment, as more carefully discussed in [1], bulk damage is modeled by considering two deep levels, the dominant "acceptor" level being related to the divacancy VV(-/0) complex, and the dominant "donor" level to the C_iO_i complex. This allows for accurate rendering of the internal carrier distribution: as discussed in [8, 9, 10], such investigations show that a steep potential drop actually survives close to the implant region, coming from a non uniform distribution of trapped and mobile charge. Thus, the overhang can still be suitably envisaged as a beneficial mean to reduce breakdown risks.

A quantitative estimate of such an action can again be obtained from Fig. 10, in which the peak field sensitivity to the overhang extension is reported, for a given geometrical configuration and at different radiation fluences. From this plot, it turns out that actually the peak amplitude even increases with the fluence: such an increase can be interpreted by referring to the increasing amount of oxide-trapped charge, which is responsible for a denser surface accumulation of electrons. Such a charge layer, acts on the field distribution by compressing equipotential lines in the narrow gap between the strip implant and the layer itself. As shown above, the overhang helps in this case too, by locally suppressing such a layer. This behavior is indeed confirmed by actual measurements: in particular, as reported in [11], a significant reduction of the breakdown voltage has been obtained with overhanging electrodes, especially for heavily irradiated structures; for these reasons, the use of metal overhang has been recently assumed as a baseline design indications for detectors to be installed at the inner tracker of CERN CMS experiment [12].

Finally, it could be mentioned that further studies (which will be discussed elsewhere) are being carried out, aimed at characterizing the sensitivity of noise parameters (mainly the interstrip capacitance) on the overhang extension. Preliminary results suggest that no significant drawbacks to the adoption of relatively wide overhang should be expected.

4 Conclusions

In this paper, a numerical study has been discussed, describing the behavior of "overhanging metal" structures implemented in silicon microstrip detectors.

Such geometries have been proposed to mitigate the impact of early micro-discharge and breakdown phenomena within irradiated structures. By means of the simulation, such an attitude has been verified and characterized: in particular, the CAD tool made it possible to look at internal field and carrier distributions, allowing for the physical interpretation of several interacting phenomena and illustrating the correlation between the overhang efficiency and the main geometrical parameters. Irradiated detectors have been analyzed as well, showing that breakdown risks are significantly lowered by the overhang in this case too.

References

[1] D. Passeri, P. Ciampolini, G.M. Bilei, "A comprehensive analysis of low-resistivity radiation detectors," *IEEE Trans. on Nuclear Science*, vol. 46, n.3, pp. 260-265, June 1999.

[2] CMS Collaboration, "CMS Technical Design Report," CERN, Ginevra, Switzerland, May 1998.

[3] T. Ohsugi *et al.*, *Nucl. Instr. and Meth.*, vol. A383, pp. 116-122, 1996.

[4] G. Baccarani, P. Ciampolini, A. Pierantoni, "Three-dimensional simulation of semiconductor devices: state of the art and prospects," *Nucl. Instr. and Meth.*, vol. A326, pp. 253-259, 1993.

[5] D. Passeri, P. Ciampolini, M. Baroncini, A. Santocchia, G.M. Bilei, B. Checcucci, E. Fiandrini, "Comprehensive Modeling of Silicon Microstrip Detectors," *IEEE Trans. on Nucl. Sc.*, vol. 44, n. 3, pp. 598-605, 1997.

[6] D. Passeri, M. Baroncini, P. Ciampolini, G.M. Bilei, A. Santocchia, B. Checcucci, E. Fiandrini, "TCAD-Based Analysis of Radiation-Hardness in Silicon Detectors," *IEEE Trans. on Nucl. Sc.*, vol. 45, n. 3, 1998.

[7] E. Fretwurst, V. Eremin, H. Feick, J. Gerhardt, Z. Li, G. Lindstrom, "Investigation of damage-induced defects in silicon by TCT," *Nucl. Instr. and Meth.*, vol. A388, pp. 356-360, 1997

[8] D. Passeri, P. Ciampolini, G.M. Bilei, G. Casse, F. Lemeilleur, "Analysis of the transient response of LED-illuminated diodes under heavy radiation damage," *Proc. of 1st ENDEASD Workshop*, Santorini, Greece, April 21-22 1999.

[9] G.Casse, E. Grigoriev, F. Lemeilleur, M. Glaser, "Study of the active volume in irradiated silicon detectors," *Proc. of 2nd Int. Conf. on Radiation Effects on Semiconductor Materials, Detectors and Devices*, Florence (Italy), March 4-6, 1998.

[10] D. Passeri, P. Ciampolini, G.M. Bilei, "A CAD investigation of depletion mechanisms in irradiated silicon microstrip detectors," *Nuclear Instruments and Methods in Physics Research*, vol. A 426, no. 1, pp. 131–134, 1999.

[11] N. Demaria, "New result on Silicon Microstrip Detectors of CMS Tracker," *8th International Workshop on Vertex Detectors*, Texel, Netherlands, 20-25 June 1999.

[12] N. Demaria, "Milestone on sensor definitions," *CMS Silicon Tracker Week meeting* CERN, Ginevra, Switzerland, 15 October 1999.

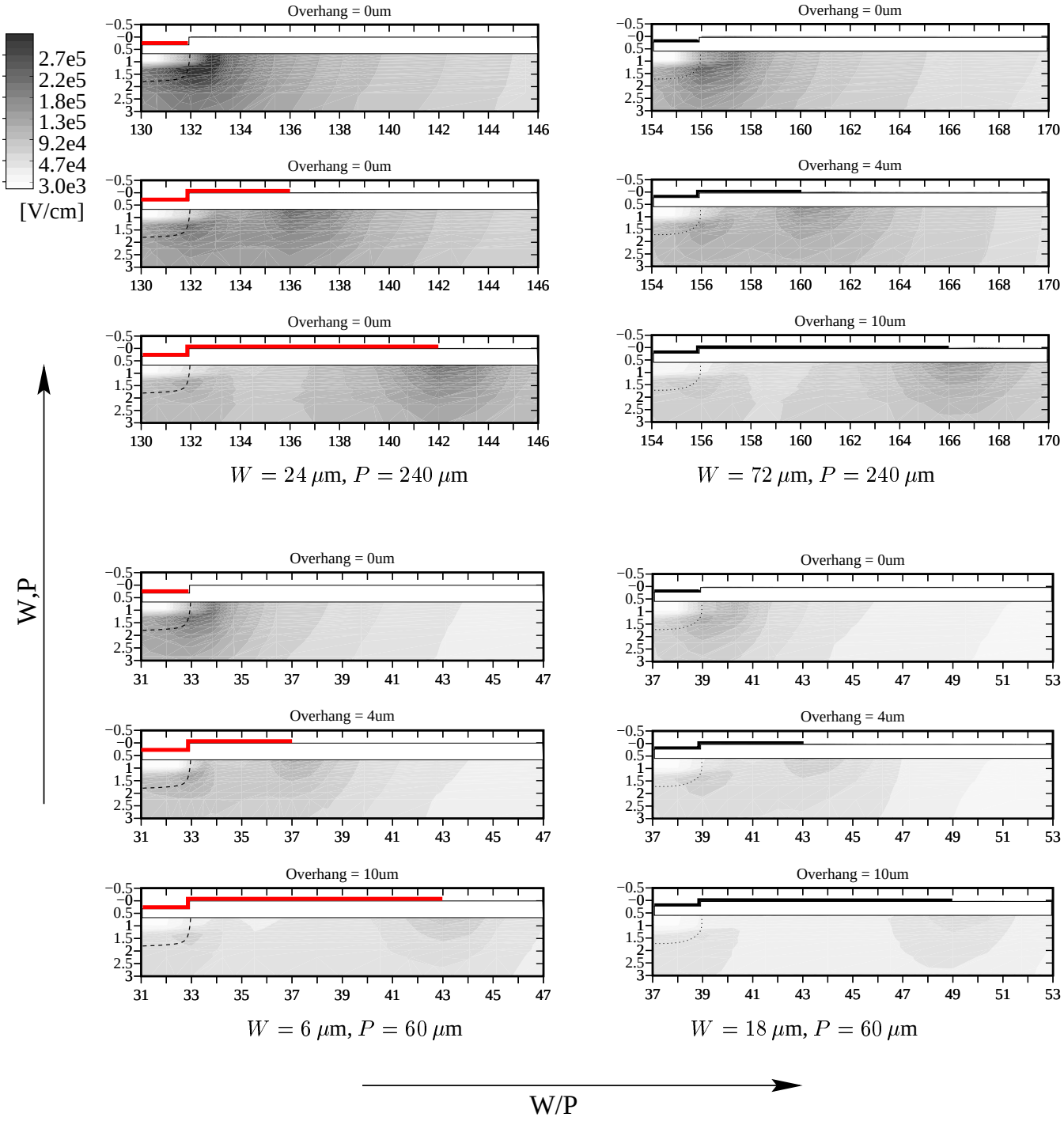

Figure 5: Electric field amplitude contour plot, depending on the strip width W, the pitch P and the overhang extension. $V_{\text{bias}} = 500$ V.

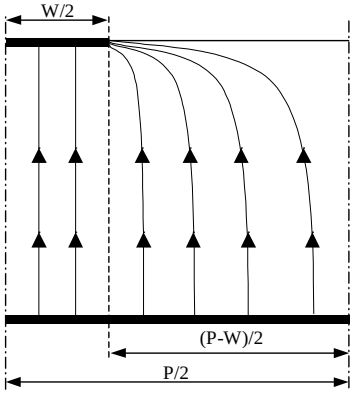

Figure 6: Schematic drawing of the fringing field lines.

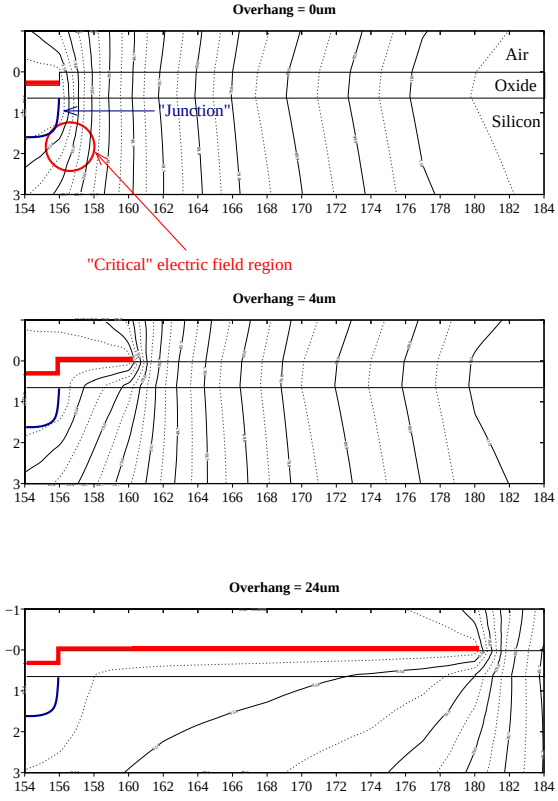

Figure 7: Potential contour plots, for different overhang extensions (implant width=72 μm, pitch=240 μm, V_{bias}=250V.

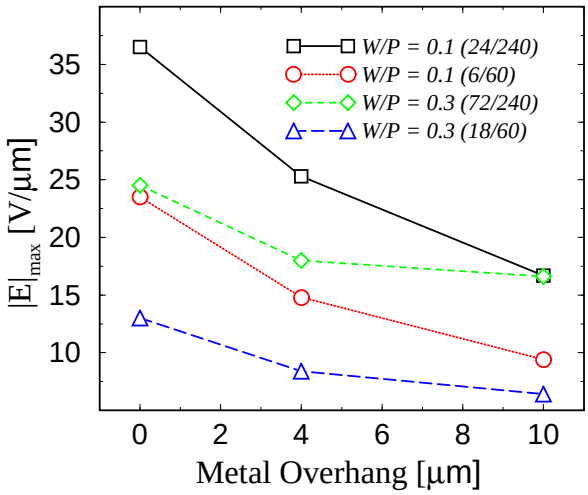

Figure 8: Electric field reduction for different geometrical configuration (V_{bias}=500V).

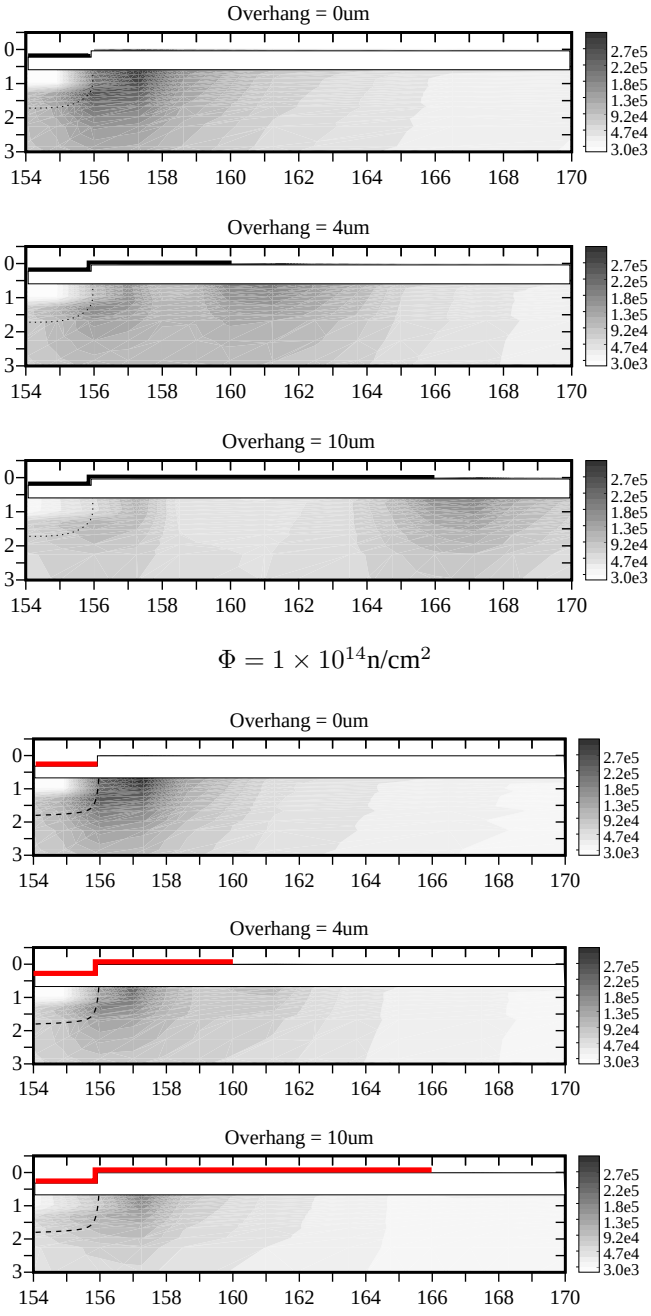

$\Phi = 1 \times 10^{14}$n/cm^2

$\Phi = 2 \times 10^{14}$n/cm^2

Figure 9: Implant width=72 μm, pitch=240 μm, V_{bias}=500V.

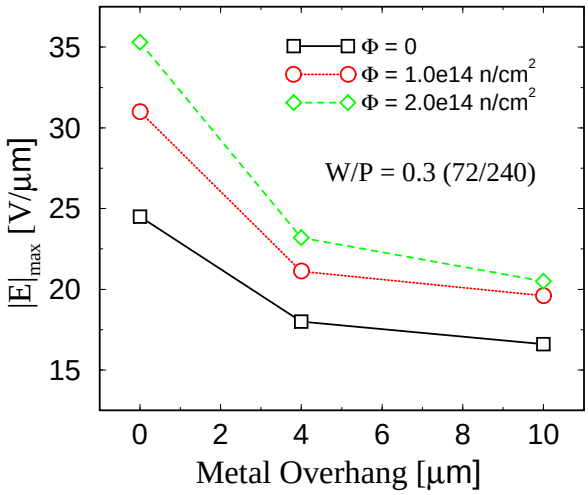

Figure 10: Electric field reduction at different radiation fluences (V_{bias}=500V).